Int. J. Nanosci. Nanotechnol., Vol. 16, No. 1, March 2020, pp. 35-48

Synthesis of Magnetic Graphene Oxide Nanocomposite for Adsorption Removal of Reactive Red 195: Modelling and Optimizing via Central Composite Design

Zahra Monsef Khoshhesab[1], Zahra Ayazi[2,*] and Maryam Dargahi[1]

[1]Department of Chemistry, Payame Noor University, Tehran, Iran.
[2]Department of Chemistry, Faculty of Sciences, Azarbaijan Shahid Madani University, P.O. Box 53714-161 Tabriz, Iran.

(*) Corresponding author: ayazi@azaruniv.edu
(Received: 17 January 2018 and Accepted: 08 August 2019)

Abstract

In this work, magnetic graphene oxide (MGO) was prepared by in situ synthesis of magnetite nanoparticles in the presence of graphene oxide (GO). The prepared nanocomposite was characterized by applying scanning electron microscopy (SEM), X-ray diffraction (XRD, Fourier transform infrared spectroscopy (FTIR) and vibrating sample magnetometer (VSM). MGO was applied as an efficient nano-sorbent for adsorptive removal of reactive red 195 (RR195). The adsorptive removal process of RR195 was modeled and optimized using the response surface methodology (RSM) based on central composite design (CCD). Important parameters influencing the adsorption of RR195 including pH, contact time, initial concentration of RR195 and adsorbent amount were selected as input variables for RSM. The highest adsorption capacity of MGO sorbent (77.2 mg g^{-1}) was obtained at an initial dye concentration of 325 mg L^{-1}, contact time of 65 min, adsorbent amount of 89.4 mg, and pH of 3. Moreover, the adsorption isotherms and kinetics studies were performed, indicating that the adsorption process best fitted in pseudo-second-order model and Langmuir isotherm model, in which the maximum adsorption capacity, q_m, was calculated to be 80 mg g^{-1}.

Keywords: *Magnetic Graphene Oxide Nanocomposite; Reactive Red 195; Central Composite Design; Adsorption Removal.*

1. INRODUCTION

In the recent decades, contamination and pollution of surface waters and waste-waters due to the extensive usage of pigments and dyes in various industries such as textile, paper and pulp is a great environmental issue and is attracting more and more attention. Large amount of pollutants are introduced into river waters and wastewaters due these industries activity. Water resources pollution not only makes the water unusable, but also causes to environmental adverse effect. The dye contaminations in water can disturb the penetration of light into the water and as a result, photosynthesis is considerably hindered [1-4]. The toxic effect of dye pollution on plants, animals and human health is not well-known. The presence of reactive groups such as oxygen, nitrogen, sulfur and halogen in the structure of azo dyes make them capable to bind covalently with other materials through amino group of polyamides, hydroxyl group of cellulose and hydroxyl, amino or mercaptan groups of proteins [5]. RR195 is a sulfonate azo dye belonging to the class of anionic reactive azo dyes which is widely used in textile industry to dying the cellulose fibers. Considering the diverse effect of dyes in environment, dye removal from effluents produced by various industrial is an important requirement to produce a safe and clean environment [6-8]. A variety of physical and chemical water treatment

methods including ozonation, membrane separation, electrochemical methods, adsorption and photo-oxidation have been employed. Among them, water treatment procedure based on adsorption is commonly used because of its unique advantages such as versatility of adsorbents, their non-toxicity, high adsorption capacity, high removal percentage and regenerability of adsorbent [9].

Nowadays, nanomaterial owning specific chemical and physical properties exhibit unique surface activity due to their high surface areas and presence of various surface atoms which can strongly interact with many chemical species. Nanocomposite (NC) materials can be considered as good candidates for chemisorption of various organic compounds (because of enhanced reactive atoms type and number on the NC surface), leading to their efficient removal [10-14]. Carbon-based materials are widely applied in the water treatment procedures based on adsorption [15, 16]. Graphene or graphene oxide (GO) materials are considered as promising materials for the adsorptive removal of the dye contaminations from the wastewaters [17-19]. Graphene exhibiting superior properties, including large specific surface area (calculated to be 2,630 $m^2\ g^{-1}$), high chemical stability, and graphitized planer structure, can establish strong π–π interactions with the various contaminant species containing aromatic moieties [20-22]. Therefore graphene can be regarded as a good adsorbent for dye removal. However, agglomeration and restacking of graphene during application, due to the π–π interactions between neighboring nanosheets cause to great decrease of effective surface area and consequently limit the adsorption efficiency [20]. Therefore, GO can be applied as an alternative for graphene, leading to the better results. Single-layered GO nanosheets can be achieved by exfoliation of graphite oxide through ultrasonication. GO because of its high water solubility, large specific surface area and presence of diverse surface functionalities such as hydroxyl, carboxylic, carbonyl and epoxide groups is a material of great interest in the methods based on adsorption as well as in other fields [23, 24]. GO can interact electrostatically with the ionic adsorbates, making it an efficient material for adsorption of charged species [18, 25]. However, the high dispersibility of GO in aqueous solutions and its small particle size are the main problems in GO application leading to its difficult separation from solution after adsorption process through centrifugation or filtration. The preparation of magnetic nanoparticle-based NC can overcome to this drawback, causing to the simple and fast separation of adsorbent after adsorption process. Applying super-paramagnetic Fe_3O_4 (magnetite), magnetic separation is more convenient, efficient, and economic, making it more interesting in divers applications [26-28]. Magnetic separation can achieve better separation efficiency with less energy especially for adsorbents with small particle size in comparison to traditional methods, such as centrifugation and filtration. Hence, preparation of magnetite/graphene oxide (MGO) NC suggests an effective solution to overcome the separation problems attributed to GO. On other hand, incorporation of the Fe_3O_4 nanoparticles can prevent the aggregation and restacking of the graphene nanosheets, leading to a higher surface area and enhanced adsorption efficiency.

In this work, MGO NC was prepared by in situ co-precipitation of magnetite nanoparticles in the presence of GO. The prepared NC was used for adsorption removal of RR195 from aquatic media. In order to investigate the effect of influencing parameters on the removal percentage and modeling the removal efficiency as a function of influencing parameters, central composite design was used. The influential factors including the contact time, initial RR195 concentration, pH and MGO mass was considered as

input variables for RSM. Finally, isothermal behavior and kinetic studies on the adsorption of RR195 were investigated.

2. EXPERIMENTAL

2.1. Reagents and Chemicals

Chemicals including ferrous chloride tetrahydrate ($FeCl_2 \cdot 4H_2O$), ferric chloride hexahydrate ($FeCl_3 \cdot 6H_2O$), ammonium hydroxide, sulfuric acid, sodium hydroxide and hydrochloric acid were all purchased from Merck (Germany). Graphite fine powder was supplied by Loba Chemie (Mumbai, India). Sodium nitrate and hydrogen peroxide (30% v/v) were obtained from Loba Chemie. Distilled water was used in all of the experiments. An anionic azo dye Reactive red 195 (RR195) also known as Reactive Brilliant Red M-3BE ($C_{31}H_{19}ClN_7O_{19}S_6\ Na_5$, M.W: 1133.36 g mol^{-1}) was purchased from Dyestar Co. (Germany).

2.2. Instruments

The concentration of RR195 was determined applying a Shimadzo UV-Vis spectrophotometer (1600 IPC, Tokyo, Japan) at λ_{max} = 542 nm wavelength. An ultrasonic cleaner (Bandelin D-12207, Germany) was used for preparation MGO NC. The solution pH was adjusted using a Metrohm 827 pH-Ion meter (Switzerland). Sample agitation was carried out using a shaker (Sahand.T.a., Iran). In order to magnetically separation of nano-sorbent from solution, a permanent magnet of Nd–Fe–B (8.0 cm × 6.0 cm × 1.6 cm) was applied. The morphological and surface characteristic of the prepared NC was studied applying scanning electron microscope (SEM) (PHILIPS XL30, Netherland). Fourier transform infrared spectroscopy (FTIR) was used to study the MGO NC applying a JASCO 4200 FTIR instrument. A PHILIPS, PW1800 (Netherland) X-ray diffractometer was used to record the X-ray diffraction pattern of prepared nano-sorbent.

Magnetic characterization of the prepared nanocomposite was performed using vibrating sample magnetometer (VSM) MDKFD instrument (Iran).

2.3. Preparation of Graphene Oxide

The preparation of GO was performed as the same method as our previous work [19], based on Hummers and Offeman method [29]. First, 3.75 g sodium nitrate and 5 g of graphite powder were added to a 500 mL flask. Next, 150 mL sulfuric acid was added to the flask and the resulted mixture was placed into an ice bath and agitated on a stirrer at 1200 rpm. Afterward, 20 g $KMnO_4$ was added slowly with stirring during 1 h. Then, the obtained mixture was stirred in ice bath for further 2 h. Then the flask was removed from the ice bath and the mixture was stirred for 3 day in room temperature. Afterward, 500 mL distilled water was added slowly to this mixture kipping the flask into the ice bath. After distilled water addition, 15 mL of hydrogen peroxide 30% was added. In order to purify the prepared GO, the mixture was washed by rinsing and centrifugation with HCl (5% v/v) followed by deionized water for several times. The obtained precipitate was dried in an air oven at 50˚C for 72 h.

2.4. Preparation of Magnetite/Graphene Oxide NC

Magnetite/graphene oxide NC was prepared through chemical co-precipitation of magnetite nanoparticles in the GO media. In a typical experiment, 1 g GO was added to 50 mL of water and placed in ultrasonication bath for 10 min for exfoliating GO nanosheet. Then, 1.25 g of $FeCl_2 \cdot 4H_2O$ and 3.5 g $FeCl_3 \cdot 6H_2O$ were added to 50 mL water and the obtained mixture was sonicated for 5 min. 150 mL water was added into the 500 mL three-necked flask and it was placed into an oil bath, kipping the temperature at 70˚C. Next, the two prepared solutions that containing GO and magnetite nanoparticles were added into flask under a nitrogen stream. Then, in order to synthesis of magnetite nanoparticles, the pH of solution

was increased up to 10 by dropwise adding 8 mL of ammonia solution (28%) to the prepared mixture. The synthesis of Fe_3O_4 nanoparticles was allowed to be completed during 45 min and then, the resulted black precipitate was removed from solution by employing an external magnetic field. For purification of prepared MGO, it was washed with water several times, and finally it was placed in an oven at 50˚C for 24 h.

Table 1. *Actual and coded values of independent variables applied for response surface method.*

Effect	**Symbol**	**-α**	**-1**	**0**	**+1**	**+α**
pH	X_1	3	4.5	6	7.5	9
Sorbent amount (mg)	X_2	0.05	0.075	0.1	0.125	0.15
Dye concentration (mg L^{-1})	X_3	25	100	175	250	325
Contact time (min)	X_4	5	20	35	50	65

2.5. Batch Adsorption Experiments

For evaluating the adsorption capability of prepared MGO NC towards RR195, batch adsorption experiments were performed by adding different amount of adsorbent into 25 mL dye solution at concentration level of 200 mg L^{-1}. The solution of 1 M HCl or 1 M NaOH was added to the dye solution in order to adjust the initial pH of the solution using a pH meter. The solutions were agitated on a shaker at room temperature for desired time. Finally, the dye loaded MGO was separated from solution by applying the external magnetic field. The concentration of RR195 in the remaining solution and initial solution was determined by UV-Vis spectrophotometric method using maximum wavelength value of 542 nm. The dye removal percentages (R%) was calculated considering the initial and final dye concentration applying the following equation (Eq (1)):

$$R\% = \frac{C_0 - C_t}{C_0} \times 100 \qquad \text{Eq. (1)}$$

in which, C_0 (mg L^{-1}) is the initial dye concentration and C_t (mg L^{-1}) is the dye concentration after time t.

For studying the adsorption kinetic and adsorption isotherms, the related parameters including equilibrium adsorption capacity (q_e, mg g^{-1}) and adsorption capacity at certain time (q_t, mg g^{-1}) were calculated using following equations (Eqs (2) and (3)):

$$q_e = \frac{(C_0 - C_e)V}{W} \qquad \text{Eq. (2)}$$

$$q_t = \frac{(C_0 - C_t)V}{W} \qquad \text{Eq. (3)}$$

where V (L) is the solution volume and W (g) is the weight of adsorbent.

2.6. Central Composite Design

In order to response modeling and optimization, RSM based on CCD was employed. In this regard, four parameters affecting the removal efficiency (k=4) have been selected as CCD factors including pH, initial concentration of RR195, contact time and adsorbent amount. Table 1 presents the coded and actual values of selected factors in the designed CCD. The MGO adsorption capacity towards RR195 (q) was considered as the model response. Considering four input variables for CCD for investigating the removal process, the designed experiments consists in 31 experiments including 16 (2^k) orthogonal full factorial design points (coded by value of ±1), 8 (2k) star or axial points (±α = 2.0) and 7 replications in the central point (coded as 0) to estimate the experimental error variance. The design of experiments and the analysis of obtained experimental data were performed using Minitab 15 software. In order to evaluate the obtained model, analysis of variance (ANOVA) was employed. The significance of the obtained polynomial regression equation was evaluated statistically by F-test and lack of fit (LOF) test. The confidence level of 95% was regarded to evaluate the significance

of the model and model terms, therefore, the P-values less than 0.05 were considered to be statistically significant.

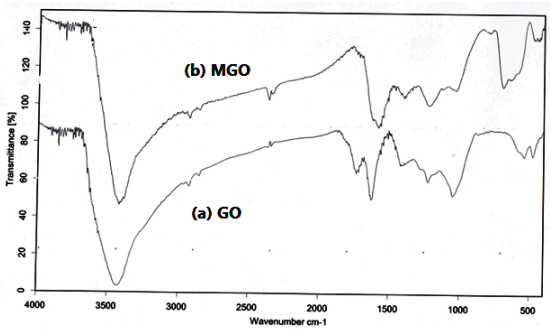

Figure 1. *FTIR pattern of (a) GO and (b) MGO.*

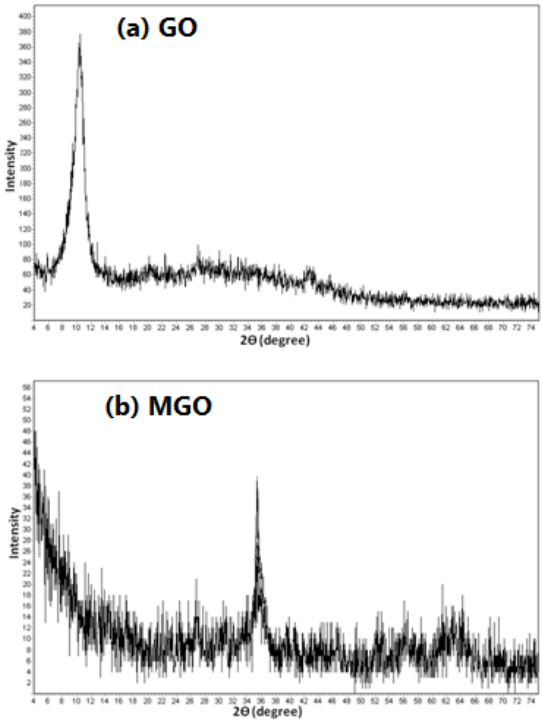

Figure 2. *XRD spectra for (a) GO and (b) MGO.*

3. RESULTS AND DISCUSSION

3.1. Characterization of Prepared MGO

In order to study and characterize the prepared MGO, FTIR, XRD and SEM was applied. FTIR spectra for the GO and MGO nanocomposite were recorded and are presented in Fig. 1. As can be seen in the FTIR spectrum of GO and MGO, there are absorption peaks at 3401 cm^{-1}, 1721 cm^{-1}, 1225 cm^{-1}, 1520 cm^{-1} and 1046 cm^{-1} relating to the O-H starching vibration, C=O stretching vibration (carboxyl and carbonyl groups), C-OH stretching vibration, aromatic ring C=C vibration and

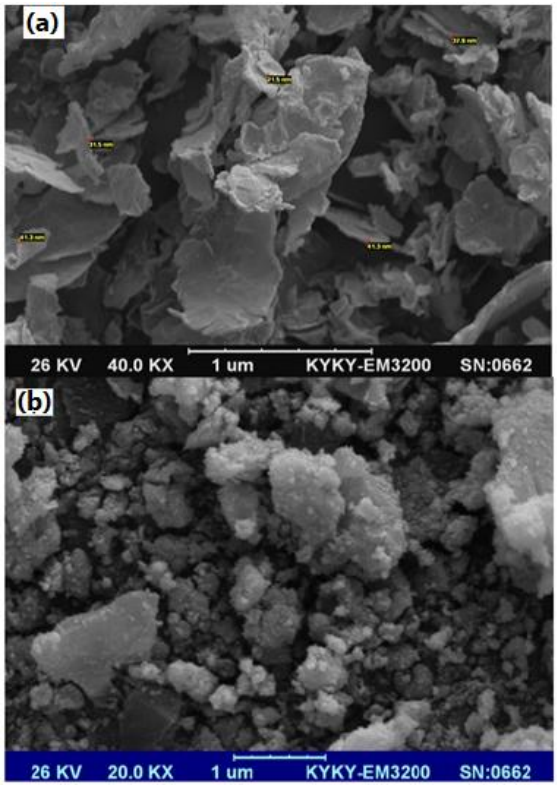

Figure 3. *SEM images of (a) GO and (b) MGO.*

epoxy O-C-O vibration, respectively [25]. The presence of epoxy, carboxyl and alkoxyl functional groups in GO and MGO was confirmed by observation of these peaks. In FTIR spectrum of MGO more absorption peaks are observed at 578 cm^{-1}, attributed to the Fe–O stretching vibration, confirming the successfully anchoring of Fe_3O_4 NPs onto GO nanosheet [26].

XRD study was also performed for GO and MGO in order to obtain the structural information about them (Fig. 2).

According to the XRD spectrum of the GO, one well defined peak at $2\theta = 10.9^{\circ}$ is observed. Considering the XRD pattern of MGO NC, one diffraction peak at $2\theta = 35.5^{\circ}$ was observed related to the diffraction of (311) for magnetite nanoparticles. Furthermore, it is evident that, the characteristic peak of GO located at 10.9° disappeared, proving the presence

of Fe_3O_4 nanoparticles on the GO nanosheets surface and disordered structure for GO [30].

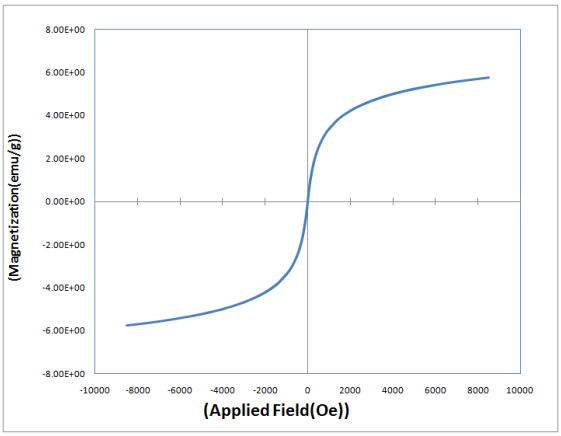

Figure 4. *Magnetization vs. applied magnetic field for magnetic graphene oxide.*

The morphological and surface characteristics of prepared GO and MGO was investigated applying SEM and the obtained SEM micrographs are presented in Fig. 3. As it is displayed in Fig. 3(a), the nanosheets of GO was clearly observed with various size and shape and same thickness. The SEM image of MGO NC (Fig. 3(b)) shows that, the Fe_3O_4 nanoparticles are anchored to the surface of the GO nanosheets. Evidently, the attached magnetite nanoparticles have nano-scale and they are well distributed throughout the prepared MGO NC.

Vibrating sample magnetometer was applied to study the magnetic character-ization of the prepared nanocomposite at room temperature, applying a magnetic field in the range of -8000 to 8000 Oe and the related parameters as coercive field (H_c) and saturation magnetization (M_s) were evaluated. Coercivity or coercive force is the force required to remove the residual magnetism from the material. VSM plot of MGO at recorded at 300 K is shown in Figure 4. The hysteresis loop does not display magnetic remanence, and thus the nanoparticles are considered to be super-paramagnetic (H_c=0 Oe). The magnetization saturation (M_s) of the MNPs was 5.76 emu g^{-1}. Accordingly, it can be concluded that the prepared MGO is superparamagnetic without coercivety and also has magnetic characteristic for separation of nanocomposite from aquatic media.

Table 2. *Estimated model coefficients for dye removal process and adsorption capacity of MGO as response and corresponding T and P values.*

Term	Coefficient	T-value	P-value	Remarks
b_0	29.4139	23.864	0.000	-
b_1	-0.4677	-0.703	0.492	-
b_2	1.5360	2.308	0.035	S[a]
b_3	5.1708	7.768	0.000	HS[b]
b_4	4.5239	6.796	0.000	HS
b_{11}	0.0116	0.019	0.985	-
b_{22}	-1.4498	-2.377	0.030	S
b_{33}	-2.4064	-3.946	0.001	HS
b_{44}	-1.4398	-2.361	0.031	S
b_{12}	2.6855	3.294	0.005	HS
b_{13}	-1.0855	-1.332	0.202	-
b_{14}	-1.2769	-1.566	0.137	-
b_{23}	1.8150	2.226	0.041	S
b_{24}	-0.5129	-0.629	0.538	-
b_{34}	1.9045	2.336	0.033	S

[a] significant at confidence level of 95% and [b] Highly significant at confidence level of 99%.

3.2. Development of RSM Model

In order to describe the removal percentage of Reactive Red 195 from aquatic media applying MGO sorbent, the regression model considering the coded values for variables can be written as following equation (Eq (4)):

$$Y = 29.4139 - 0.4677x_1 + 1.5360x_2 + 5.1708x_3 + 4.5239x_4 + 0.0116x_1^2 - 1.4498x_2^2 - 2.4064x_3^2 - 1.4398x_4^2 + 2.6855x_1x_2 - 1.0855x_1x_3 - 1.2769x_1x_4 + 1.8150x_2x_3 - 0.5129x_2x_4 + 1.9045x_3x_4 \quad \text{Eq. (4)}$$

Where, x_1, x_2, x_3 and x_4 are pH, sorbent amount, dye concentration and contact time, respectively.

In order to rewrite the final regression model, the significance of each term

should be evaluated and consequently, the insignificant parameters should be omitted and significant parameters should be remained in the regression model. Therefore, the significance of each term in the obtained regression model was carried out considering the corresponding Student's t values and P-values (Table 2). For an important and significant coefficient the T-value should be greater and/or the P-value should be less than 0.05 at 95% of significance [31]. Considering the data represented in the Table 2, the insignificant coefficient in Eq. (4) (the coefficient with P-value greater than 0.05) were eliminated and the mentioned equations were rewritten as Eq. (5).

$$Y = 29.4139 + 1.5360x_2 + 5.1708x_3 + 4.5239x_4 - 1.4498x_2^2 - 2.4064x_3^2 - 1.4398x_4^2 + 2.6855x_1x_2 + 1.8150x_2x_3 + 1.9045x_3x_4 \quad \text{Eq. (5)}$$

As represented in Eq. (5), the regression model of removal process of RR195 consisted in three main effects, three interaction effects and three curvature effects. In order to estimate the effect of each parameter on the response, the percentage effect of each parameter on the response can be calculated using Pareto analysis as the follows (Eq. (6)) [31]:

$$P_i = \frac{b_i^2}{\sum_{i=1}^{n} b_i^2} \times 100 \quad \text{Eq. (6)}$$

where P_i and b_i are the percentage effect of each term and the corresponding coefficient, respectively. The results of Pareto analysis (Fig. 5) indicates that, the most effective parameters is the main effect of dye concentration (b_3, 34.75 %). The second important term is contact time (b_4, 26.60%). Initial concentration of dye is one of the important factors affecting the adsorption capacity with positive sign, which its effect can be displayed by Pareto analysis and response surface plot (Fig. 6). As it can be seen in Fig. 4b, 4d and 4f, dye initial concentration has a positive effect on adsorption capacity, showing the increase of adsorption capacity by increase of the dye concentration. Higher adsorption capacity at higher dye initial concentrations, is might be due to the

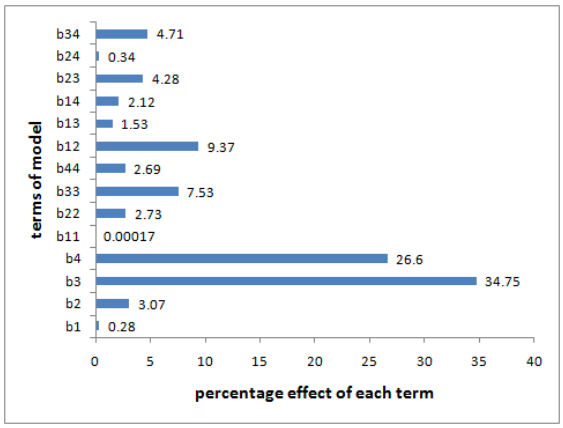

Figure 5. *Percentage effect of each model term obtained using Pareto analysis.*

saturation of adsorptive sites on the surface of MGO NC.

The contact time is another important factor influencing the adsorption capacity, which its main effect has positive sign, indicating the increase of adsorption capacity with the increase of exposure time. This is attributed to the increase of adsorbed species onto MGO sorbent during the longer contact time.

Sorbent amount is shown as less effective factor with positive sign which indicates the increase of adsorption capacity with increase of sorbent dosage (Fig. 6a, 6d and 6e). As resulted, the main effect of pH is not significant, while its interaction effect with sorbent amount is significant (Table 2 and Fig. 6a). At lower sorbent amount, the increase of pH value from 3 to 9, the adsorption capacities was decreased, due to the deprotonation of hydroxyl and carboxyl groups of MGO and consequently decreases of electrostatic interaction between sorbent and anionic dye. While, applying higher sorbent mass, the increase of solution pH shows adverse effect on adsorption capacity, which is might be due the higher amount of adsorption sites available for adsorbing the anionic RR195.

3.3 Evaluation of Quality and Significance of Regression Model

The evaluation of adequacy and significance of the developed regression model was performed through analysis of variance (ANOVA) and the corresponding results are tabulated in Table 3. Lack of fit (LOF) test and Fisher's variance ratio test (F-test) were applied to evaluate the significance and quality of the second-order regression model. Considering the results presented in Table 3, the Fisher F-values of regression is 11.53, which is much higher than the tabulated F-value at significance level of 95% (2.352), indicating the suitable prediction of experimental results by regression model. Furthermore, P-values of regression is 0.000, which is much lower than 0.05 (at the significance level of 95%), confirming the statistically significance of the regression model [31]. Additionally, lack of fit test was conducted by comparing the residuals with obtained pure error from replication of experiment in central point [32]. For this purpose, the lower F-value of LOF and/or greater P-value than 0.05 confirms the adequacy and significance of regression model. According to the data in Table 2, the P-value of LOF test was 0.094, indicating the insignificant lack of fit.

Furthermore, in order to evaluate the significance of regression model graphically, residuals can be used. Residuals are unexplained variations by model and if the model would be good predictor they have a normal distribution behavior. The normal probability versus internally studentized residuals was illustrated in Fig. 7a. Accordingly, no considerable dispersal for the obtained data points was observed and as expected the normal probability plot is in form of relatively straight line. Moreover, plots of residuals versus predicted adsorption capacity of sorbent and versus order of experiments (Fig. 7b and Fig. 7d) show the random distribution of the residuals, indicating the good fitness between experimental data and predicted adsorption capacity. In addition, the histogram of residuals was illustrated in Fig. 7c shows rather normal distribution of residuals.

3.4. Numerical Optimization

For this purpose, the values of selected factors were set to the experimental ranges, while the model response (adsorption capacity) was considered to be the maximum value. Hence, the highest adsorption capacity of MGO sorbent (77.2 mg g^{-1}) was obtained at an initial dye concentration of 325 mg L^{-1}, contact time of 65 min, adsorbent amount of 89.4 mg, and pH of 3. In order to examine the model prediction ability, confirmatory experiment was conducted applying the suggested optimum condition for dye removal. According to the obtained data, the adsorption capacity of sorbent under optimum condition was calculated to be 80, which proved the accuracy of predicted response by the regression model.

Table 3. *Analysis of variance (ANOVA) for the developed model.*

Source	DF	Seq SS	Adj SS	Adj MS	F -value	P-value
Regression	14	1716.89	1716.89	122.635	11.53	0.000
Linear	4	1194.76	1194.76	298.689	28.09	0.000
Square	4	246.84	246.84	61.711	5.80	0.004
Interaction	6	275.29	275.29	45.881	4.31	0.009
Residual error	16	170.15	170.15	10.634	-	-
Lack-of-fit	10	141.95	141.95	14.195	3.02	0.094
Pure error	6	28.19	28.19	4.698	-	-
Total	30	1887.03	-	-	-	-

[a] Degree of freedom.
[b] Sum of squares.
[c] Adjusted mean square

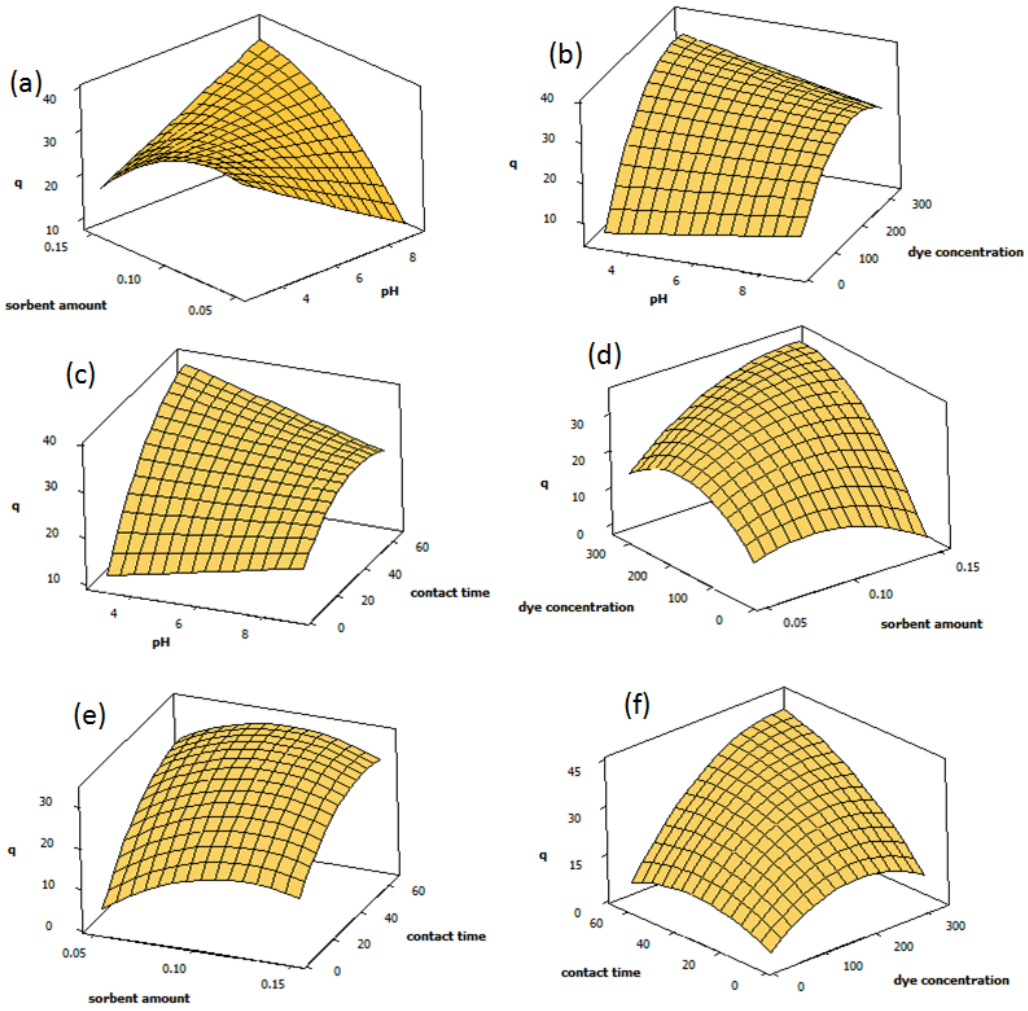

Figure 6. *Response surface plots of predicted MGO adsorption capacity towards RR195 as a function of (a) pH and sorbent amount, (b) pH and dye concentration, (c) pH and contact time, (d) sorbent amount and dye concentration, (e) sorbent amount and contact time and (f) dye concentration and contact time, keeping other variables at central point levels.*

Table 4. *Adsorption kinetic parameters for RR195 adsorption onto 89.4 mg of MGO in 25 mL RR195 solution at pH of 3 and room temperature.*

Pseudo-first-order kinetic	K_1	Rate constant of pseudo-first order adsorption (L min^{-1})	0.018
	q_e (cal)	Equilibrium capacity (mg g^{-1})	28.25
	R^2	Correlation coefficient	0.858
Pseudo-second-order kinetic	k_2	Second-order rate constant of adsorption (g $(mg\ min)^{-1}$)	0.00198
	q_e (cal)	Equilibrium capacity (mg g^{-1})	80
	R^2	Correlation coefficient	0.9999
q_e (exp)		Experimental data of the equilibrium capacity (mg g^{-1})	79.93

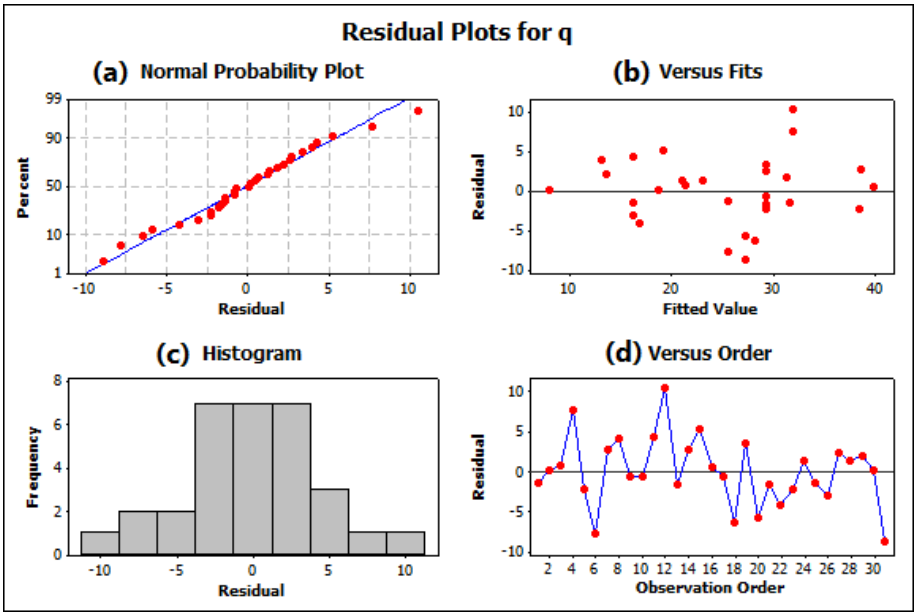

Figure 7. *Residual plots for adsorption capacity of MGO towards RR195 (a) normal probability plots of residuals, (b) residuals versus fits plots, (c) histogram of residuals and (d) residuals versus observation order.*

3.5. Adsorption Kinetics

Kinetic study for adsorptive removal process provides important information about the mechanism of adsorption. In order to estimate the kinetic adsorption constant and find the rate-controlling steps like chemisorption or diffusion process, the experimental data were evaluated applying two common and important kinetic models: pseudo-first-order model [33] and pseudo-second-order model [34] which are expressed as follows:

$$\log(q_e - q_t) = log q_e - \frac{k_1}{2.3} t \qquad \text{Eq. (7)}$$

$$\frac{t}{q_t} = \frac{1}{k_2 q_e^2} + \frac{t}{q_e} \qquad \text{Eq. (8)}$$

where, q_e and q_t have the same meaning as above mentioned, k_1 is the rate constant of the first-order model (min^{-1}) and k_2 ($g \cdot mg^{-1} \cdot min^{-1}$) is the rate constant of pseudo-second-order model. The values of k_L, q_e and correlation coefficient were evaluated from linear plots of *log* (q_e-q_t) versus *t* for the pseudo first order model. It is important to emphasize that in many instances, experimental data do not fit over the whole range of contact time with the pseudo-first-order model properly and this model only at the primary stage of adsorption applicable to experimental data. The graph of t/q_t versus *t* gives a straight line that the q_e and k_2 are evaluated from the slopes and intercepts of this line. The pseudo-second-order kinetics model is based on the assumption that the adsorption process is controlled by the pseudo-chemical reaction. The correlation coefficients, R^2, show the level of consistency between the experimental and predicted values. The higher R^2 value or the value closer to one confirms the better applicability of the model.

In order to investigate the kinetic behavior of RR195 removal applying MGO NC, 89.4 mg of adsorbent was added to the 25 mL of RR195 solution at concentration level of 325 mg L^{-1} at pH= 3 and room temperature and the adsorption process was conducted during 10 to 80 min. Table 4 presents the models correlation coefficients values (R^2) along with kinetic parameters calculated applying as mentioned kinetic models for adsorption of RR195 onto MGO NC. Accordingly, pseudo – second - order

Table 5. *Isotherm parameters and correlation coefficients calculated by various adsorption models onto 89.4 mg of MGO in 25 mL RR195 solution at pH 3 and room temperature.*

Langmuir	q_m	Maximum adsorption capacity reflected a complete monolayer (mg g^{-1})	80
	b	Langmuir constant or adsorption equilibrium constant (L mg^{-1})	0.969
	R^2	Correlation coefficient	0.9999
Freundlich	n	Isotherm constant indicate the empirical parameter (g L^{-1})	13.89
	K_F	Isotherm constant indicate the capacity parameter (mg g^{-1})	55.46
	R^2	Correlation coefficient	0.917
Temkin	B_1	Related to the heat of adsorption	5.13
	K_T	Equilibrium binding constant (L mg^{-1})	38465.03
	R^2	Correlation coefficient	0.925

adsorption mechanism exhibited higher correlation coefficients values than pseudo-first-order kinetic model. Moreover, the values of q_e*(cal)* calculated from pseudo second-order model (80 mg g^{-1}) is very closer to the obtained experimental values of q_e*(exp)* (79.93 mg g^{-1}) (Table 4). These results demonstrate that the pseudo second-order kinetic model is predominant.

3.6. Adsorption Isotherm

Adsorption isotherms provide elucidate slight for description of interaction between target compounds and adsorbent surface. Adsorption equilibrium isotherm is described according to the mathematical relation of the amount of adsorbed target species at equilibrium (q_e (mg g^{-1})) to the equilibrium non-adsorbed amount of target species remained in solution (C_e (mg L^{-1})) at constant temperature. Adsorption isotherms consist in famous models such as Langmuir [35], Freundlich [36] and Temkin [37] which have been employed for explanation of the experimental adsorption data. The Langmuir isotherm is based on the monolayer adsorption of solute onto adsorbent surface because of a finite number of identical sites. According to this model, the adsorption of adsorbates takes place on a homogenous adsorbent surface and there is no interaction between target molecules. This isotherm model is expressed in the linear form as following equation:

$$\frac{C_e}{q_e} = \frac{1}{bq_m} + \frac{C_e}{q_m} \qquad \text{Eq. (9)}$$

where C_e and q_e are as defined already. The Langmuir constants, q_m (mg g^{-1}) and b (L mg^{-1}) are related to the capacity of monolayer adsorption and the heat of adsorption, respectively.

The Freundlich isotherm assumes that the adsorption of target molecules onto the adsorbent takes place in multilayer state with the heterogeneous surface and is defined as Eq. (10):

$$lnq_e = lnK_f + \frac{1}{n} lnC_e \qquad \text{Eq. (10)}$$

where K_f (mg g^{-1}) is an estimation for the adsorption capacity, and *1/n* denote the intensity of multilayer adsorption, indicating the favorability of adsorption. The *n* values higher that unit ($n > 1$) suggests favorable adsorption condition.

Based on the Temkin isotherm equation, it is assumed that, the adsorption heat for all adsorbates in layer decreases linearly with coverage of layer due to the adsorbent-adsorbate interactions. According to this isotherm equation, the adsorption is characterized by a uniform distribution of the bonding energies, up to some maximum binding energy. The Temkin isotherm is defined in linear form as follows:

$$q_e = B_1 \ln K_T + B_1 \ln C_e \qquad \text{Eq (11)}$$

where $B_1 = RT/b$ is the heat of adsorption, in which, R and T are the universal gas constant (8.314 J mol^{-1} K^{-1}) and the

Table 6. *Comparison of MGO adsorptive performance with other reported adsorbent.*

Sorbent	Isotherm model	Kinetic model	q_e (mg g^{-1})	Contact time (min)	reference
Pinus sylvestris L	Freundlich	second-order	7.38	180	[39]
TiO_2 nanoparticles	Langmuir	pseudo-second-order	87	60	[40]
dehydrated beet pulp carbon	Freundlich	pseudo-first-order	58	200	[41]
MGO	Langmuir	pseudo-second-order	80	65	This work

absolute temperature in Kelvin, respectively [38]. K_T is the equilibrium binding constant (L mol^{-1}) corresponding to the maximum binding energy. By plotting q_e versus lnC_e, the isotherm constants B_1 and K_T can be calculated from the slope and the intercept of linear equation, respectively.

In this work, in order to evaluate the adsorption isotherms for RR195 adsorption onto MGO NC, a series of experiments was performed by adding 89.4 mg of MGO NC to the 25 ml of RR195 solutions at different concentration levels of 50 to 500 mg L^{-1} at pH of 3. After 65 min, the adsorbent was removed magnetically and consequently the concentration of RR195 in the solution was determined. The obtained data were fitted into the as discussed isotherms models via Eqs. (8) to (10) and the isotherm parameters were calculated. Table 4 represents the detailed parameters of adsorption isotherms. Accordingly, the correlation coefficient of Langmuir isotherm is higher than others, suggesting the good fitness of experimental data in Langmuir isotherm. Therefore, it can be concluded that the adsorption of RR195 onto MGO exhibited the monolayer chemisorption and homogeneous behavior. According to this model, Langmuir constant, q_m was obtained to be 80 mg g^{-1}.

3.7. Comparison of MGO Performance with Other Reported Adsorbent

The adsorptive performance of the synthesized magnetic graphene oxide was compared with other sorbents applied for removal of RR195 from aqueous solutions [39-41]. According to the data tabulated in Table 6, the adsorption capacity of the prepared MGO is higher than others adsorption capacity, except of TiO_2 nanoparticles which is similar to MGO. The equilibrium contact time was also compared for various sorbents, showing the lower contact time required to reach the equilibrium condition. Considering the high adsorption capacity and shorter equilibrium contact time, it can be concluded that the prepared MGO can be applicable candidate for removing RR195 as a representative compound of anionic azo dyes.

4. CONCLUSIONS

The MGO nanocomposite was synthesized by in situ preparation of magnetite nanoparticles in the presence of GO suspension. The prepared NC was characterized using SEM, XRD and FTIR and the obtained data confirmed the successful preparation of desired nano-sorbent. The prepared MGO NC was employed for the adsorption removal of RR195 from aquatic media. The adsorption process was modeled and optimized through batch experiments using CCD. The adsorption isotherms were studied and the obtained results revealed that experimental equilibrium data were well fitted into Langmuir model. The corresponding adsorption capacity, q_m, was calculated to be 80 mg g^{-1}. Additionally, considering the kinetic studies, it was revealed that the kinetic behavior of RR195 adsorption onto MGO NC can be well described according

to the pseudo-second-order kinetic model. Finally, it can be concluded that, the prepared MGO NC is characterized by significantly higher adsorption capability, stability, fast, simple and convenient separation from solution, suggesting this nano-sorbent as an industrially viable, economical and successful product to removal of some organic contaminant in aqueous media.

ACKNOWLEDGMENTS

The authors would like to thank the Payame Noor University (Tehran, Iran) and Research Consul of Azarbaijan Shahid Madani University (Tabriz, Iran) for their instrumental and financial supports.

REFERENCES

1. Gupta, V. K., Ali, I., Saleh, T. A., Nayak, A., Agarwal, S., (2012) "Chemical treatment technologies for waste-water recycling: an overview", *RSC Advances*, 2(16): 6380-6388.
2. Gupta, V. K., Kumar, R., Nayak, A., Saleh, T. A., Barakat, M. A., (2013) "Adsorptive removal of dyes from aqueous solution onto carbon nanotubes: a review", *Advances in Colloid and Interface Science*, 193: 24-34.
3. Khani, H., Rofouei, M. K., Arab, P., Gupta, V. K., Vafaei, Z., (2010) "Multi-walled carbon nanotubes-ionic liquid-carbon paste electrode as a super selectivity sensor: application to potentiometric monitoring of mercury ion (II)", *Journal of Hazardous Materials*, 183(1-3): 402-409.
4. Saravanan, R., Khan, M. M., Gupta, V. K., Mosquera, E., Gracia, F., Narayanan, V., Stephen, A., (2015) "ZnO/Ag/Mn_2O_3 nanocomposite for visible light-induced industrial textile effluent degradation, uric acid and ascorbic acid sensing and antimicrobial activity", *RSC Advances*, 5(44): 34645-34651.
5. Tuzen, M., Soylak, M., (2007) "Multiwalled carbon nanotubes for speciation of chromium in environmental samples", *Journal of Hazardous Materials*, 147(1): 219-225.
6. Constantin, M., Asmarandei, I., Harabagiu, V., Ghimici, L., Ascenzi, P., Fundueanu, G., (2013) "Removal of anionic dyes from aqueous solutions by an ion-exchanger based on pullulan microspheres", *Carbohydrate polymers*, 91(1): 74-84.
7. Li, W. H., Yue, Q. Y., Gao, B. Y., Ma, Z. H., Li, Y. J., Zhao, H. X., (2011) "Preparation and utilization of sludge-based activated carbon for the adsorption of dyes from aqueous solutions", *Chemical Engineering Journal*, 171(1): 320-327.
8. Ayazi, Z., Khoshhesab, Z. M., Azhar, F. F., Mohajeri, Z., (2017) "Modeling and optimization of adsorption removal of reactive orange 13 on the alginate/montmorillonite/polyaniline nanocomposite via response surface methodology", *Journal of the Chinese Chemical Society*, 64(6): 627-639.
9. Tsai, W. T., Chang, Y. M., Lai, C. W., Lo, C. C., (2005) "Adsorption of ethyl violet dye in aqueous solution by regenerated spent bleaching earth", *Journal of colloid and interface science*, 289(2): 333-338.
10. Ayazi, Z., (2017) "Application of nanocomposite-based sorbents in microextraction techniques: a review", *Analyst*, 142(5): 721-739.
11. Bagheri, H., Ayazi, Z., Aghakhani, A., (2011) "A novel needle trap sorbent based on carbon nanotube-sol-gel for microextraction of polycyclic aromatic hydrocarbons from aquatic media", *Analytica Chimica Acta*, 683(2): 212-220.
12. Khayyat Sarkar, Z., Khayyat Sarkar, V., (2018) "Removal of mercury (II) from wastewater by magnetic solid phase extraction with polyethylene glycol (PEG)-coated Fe_3O_4 nanoparticles", *International Journal of Nanoscience and Nanotechnology*, 14(1): 65-70.
13. Naeimi Bagheini, A., Saeidi, M., Boroomand, N., (2018) "Removal of diazinon pesticide using amino-silane modified magnetite nanoparticles from contaminated water", *International Journal of Nanoscience and Nanotechnology*, 14(1): 19-32.
14. Taghizade Firozjaee, T., Mehrdadi, N., Baghdadi, M., Nabi Bidhendi, G. R., (2018) "Application of nanotechnology in pesticides removal from aqueous solutions: a review", *International Journal of Nanoscience and Nanotechnology*, 14(1): 43-56.
15. Sivakumar, P., Palanisamy, P. N., (2009) "Adsorption studies of basic Red 29 by a non-conventional activated carbon prepared from Euphorbia antiquorum L", *International Journal of Chemical Technology Res*earch, 1(3): 502-510.
16. Hamidi Malayeri, F., Sohrabi, M. R., Ghourchian, H., (2012) "Magnetic multi-walled carbon nanotube as an adsorbent for toluidine blue o removal from aqueous solution", *International Journal of Nanoscience and Nanotechnology*, 8(2): 79-86.
17. Pang, X. Y., Gong, F., (2008) "Study on the adsorption kinetics of acid red 3B on expanded graphite", *Journal of Chemistry*, 5(4): 802-809.
18. Bradder, P., Ling, S. K., Wang, S., Liu, S., (2010) "Dye adsorption on layered graphite oxide", *Journal of Chemical & Engineering Data*, 56(1): 138-141.

19. Ayazi, Z., Khoshhesab, Z. M., Norouzi, S., (2016) "Modeling and optimizing of adsorption removal of Reactive Blue 19 on the magnetite/graphene oxide nanocomposite via response surface methodology", *Desalination and Water Treatment*, 57(52): 25301-25316.
20. Loh, K. P., Bao, Q., Ang, P. K., Yang, J., (2010) "The chemistry of graphene", *Journal of Materials Chemistry*, 20(12): 2277-2289.
21. Su, Q., Pang, S., Alijani, V., Li, C., Feng, X., Mullen, K., (2009) "Composites of graphene with large aromatic molecules", *Advanced materials*, 21(31): 3191-3195.
22. Ayazi, Z.Jaafarzadeh, R., (2017) "Graphene oxide/polyamide nanocomposite as a novel stir bar coating for sorptive extraction of organophosphorous pesticides in fruit juice and vegetable samples", *Chromatographia*, 80(9): 1411-1422.
23. Li, D., Muller, M. B., Gilje, S., Kaner, R. B., Wallace, G. G., (2008) "Processable aqueous dispersions of graphene nanosheets", *Nature nanotechnology*, 3(2): 101-105.
24. Park, S., Ruoff, R. S., (2009) "Chemical methods for the production of graphenes", *Nature nanotechnology*, 4(4): 217-224.
25. Ramesha, G. K., Kumara, A. V., Muralidhara, H. B., Sampath, S., (2011) "Graphene and graphene oxide as effective adsorbents toward anionic and cationic dyes", *Journal of colloid and interface science*, 361(1): 270-277.
26. Sun, J., Liang, Q., Han, Q., Zhang, X., Ding, M., (2015) "One-step synthesis of magnetic graphene oxide nanocomposite and its application in magnetic solid phase extraction of heavy metal ions from biological samples", *Talanta*, 132: 557-563.
27. Chang, Y. P., Ren, C. L., Qu, J. C., Chen, X. G., (2012) "Preparation and characterization of Fe_3O_4/graphene nanocomposite and investigation of its adsorption performance for aniline and p-chloroaniline", *Applied Surface Science*, 261: 504-509.
28. Khoshhesab, Z. M., Ayazi, Z., Farrokhrouz, Z., (2016) "Ultrasound-assisted mixed hemimicelle magnetic solid phase extraction followed by high performance liquid chromatography for the quantification of atorvastatin in biological and aquatic samples", *Analytical Methods*, 8(24): 4934-4940.
29. Hummers Jr, W. S., Offeman, R. E., (1958) "Preparation of graphitic oxide", *Journal of the American Chemical society*, 80(6): 1339-1339.
30. Zhang, M., Lei, D., Yin, X., Chen, L., Li, Q., Wang, Y., Wang, T., (2010) "Magnetite/graphene composites: microwave irradiation synthesis and enhanced cycling and rate performances for lithium ion batteries", *Journal of Materials Chemistry*, 20(26): 5538-5543.
31. Ayazi, Z., Rafighi, P., (2015) "Preparation and application of a carbon nanotube reinforced polyamide-based stir bar for sorptive extraction of naproxen from biological samples prior to its spectrofluorometric determination", *Analytical Methods*, 7(7): 3200-3210.
32. Bhatti, M. S., Reddy, A. S., Thukral, A. K., (2009) "Electrocoagulation removal of Cr (VI) from simulated wastewater using response surface methodology", *Journal of Hazardous materials*, 172(2): 839-846.
33. Largergren, S., (1898) "Zur theorie der sogenannten adsorption geloster stoffe. Kungliga Svenska Vetenskapsakademiens", *Handlingar*, 24: 1-39.
34. Rengaraj, S., Kim, Y., Joo, C. K., Yi, J., (2004) "Removal of copper from aqueous solution by aminated and protonated mesoporous aluminas: kinetics and equilibrium", *Journal of Colloid and Interface Science*, 273(1): 14-21.
35. Langmuir, I., (1918) "The adsorption of gases on plane surfaces of glass, mica and platinum", *Journal of the American Chemical society*, 40(9): 1361-1403.
36. Freundlich, H., (1906) "Uber die adsorption in losungen [Adsorption in solution]â€ Zeitschrift fur Physikalische Chemie, 57".
37. Temkin, M. J., Pyzhev, V., (1940) "Recent modifications to Langmuir isotherms".
38. Akkaya, G., Ozer, A., (2005) "Biosorption of Acid Red 274 (AR 274) on Dicranella varia: Determination of equilibrium and kinetic model parameters", *Process Biochemistry*, 40(11): 3559-3568.
39. Aksakal, O., Ucun, H., (2010) "Equilibrium, kinetic and thermodynamic studies of the biosorption of textile dye (Reactive Red 195) onto Pinus sylvestris L", *Journal of Hazardous Materials*, 181(1-3): 666-672.
40. Belessi, V., Romanos, G., Boukos, N., Lambropoulou, D., Trapalis, C., (2009) "Removal of Reactive Red 195 from aqueous solutions by adsorption on the surface of TiO2 nanoparticles", *Journal of Hazardous Materials*, 170(2-3): 836-844.
41. Dursun, A. Y., Tepe, O., (2011) "Removal of Chemazol Reactive Red 195 from aqueous solution by dehydrated beet pulp carbon", *Journal of Hazardous Materials*, 194: 303-311.